Stacking-dependent excitonic properties of bilayer blue phosphorene

F. Iyikanat,[1,*] E. Torun,[2] R. T. Senger,[1,3] and H. Sahin[3,4]
[1]*Department of Physics, Izmir Institute of Technology, 35430 Izmir, Turkey*
[2]*Physics and Materials Science Research Unit, University of Luxembourg, 162a Avenue de la Faïencerie, L-1511 Luxembourg, Luxembourg*
[3]*ICTP-ECAR Eurasian Center for Advanced Research, Izmir Institute of Technology, 35430 Izmir, Turkey*
[4]*Department of Photonics, Izmir Institute of Technology, 35430 Izmir, Turkey*

(Received 27 April 2019; revised manuscript received 24 July 2019; published 16 September 2019)

Ab initio calculations in the framework of many-body perturbation theory (MBPT) are performed to calculate the electronic and optical properties of monolayer and bilayer blue phosphorene with different stacking configurations. It is found that the stacking configuration of bilayer blue phosphorene strongly affects the electronic band gap of the material. By solving the Bethe-Salpeter equation (BSE) on top of the G_0W_0 calculation, the binding energies, spectral positions, and band decomposition of excitons of monolayer and bilayer configurations are investigated. The most prominent two excitonic peaks of bilayers are examined in detail. Our calculations show that different stacking configurations lead to distinct interlayer interaction characteristics which lead to substantial change in the optical spectrum of bilayer blue phosphorene. Mostly intralayer and mixed interlayer excitons with quite high binding energies are obtained in bilayer blue phosphorene. Our results show that excitonic properties of ultrathin materials play an important role in tuning and improving the optoelectronic performance of two-dimensional materials.

DOI: 10.1103/PhysRevB.100.125423

I. INTRODUCTION

An exciton is an electrically neutral quasiparticle composed of an electron and a hole interacting with Coulomb forces. Depending on the crystal structure of the material, the exciton binding energy may be an important physical quantity in determining the optical gap of the material. Due to small carrier effective mass and high dielectric screening, the exciton binding energy of typical bulk semiconductors is in the range of a few meV. Low-temperature absorption measurements showed that the exciton binding energy of GaAs crystal is 4.2 meV [1]. Shan *et al.* showed that the electron-hole interaction in GaN and SiC is weak and therefore it is vulnerable to thermal broadening [2].

It is known that changing the dimensionality of a semiconductor from three-dimensional (3D) to two-dimensional (2D) leads to enhancement of the quantum confinement effects and reduces the Coulomb screening. The weakly screened Coulomb interaction between electron and hole increases the exciton binding energy of 2D materials up to several hundred meV [3–5]. Therefore, excitonic effects play important roles in the optical properties of 2D materials. For instance, Ugeda *et al.* showed that many-body interactions and high exciton binding energy (0.55 eV) have a significant effect on electronic and optoelectronic properties of monolayer $MoSe_2$ [6]. Experimental studies revealed that optical gap of monolayer MoS_2 is significantly lower than the quasipaticle band gap [7,8]. Li *et al.* revealed that interband transitions of few-layer black phosphorene cover a wide spectral range from the visible to the mid-infrared [9]. Recently, Zhang *et al.* found that few-layer black phosphorene has high exciton binding energy with a strong layer dependence [10]. They predicted a high exciton binding energy of ∼800 meV for free-standing monolayer black phosphorene.

Fundamental understanding of formation of excitons is extremely important for their usage in optoelectronic devices. Previous studies reported the linear relationship between the quasiparticle band gap of a 2D material and the exciton binding energy [11,12]. Therefore, the exciton binding energy of wide-bandgap monolayers is expected to be much higher than that of the monolayer transition metal dichalcogenides (TMDs). Recently, the monolayer form of blue phosphorene was synthesized on a Au(111) surface [13–15]. It has a silicene-like atomic formation with a buckled layered structure. In a recent theoretical study the quasiparticle band gap of monolayer blue phosphorene was found to be much larger than that of monolayer TMDs, and it has a significantly high exciton binding energy [16]. Moreover it was revealed that the band gap of monolayer blue phosphorene can be altered easily by means of external stimuli [17,18]. Pontes *et al.* showed that interlayer distance of bilayer blue phosphorene strongly depends on the stacking order [19]. This feature of bilayer blue phosphorene can be exploited to engineer and manipulate excitons for the sake of optoelectronic applications.

One of the most common methods for manipulating excitonic properties in 2D materials is to create van der Waals heterostructures. Recently, it was shown that optical spectrum of heterobilayers of TMDs is significantly altered by twist-angle dependent Moiré exciton peaks [20–22]. Heterostructures can host interlayer excitons where the electron and hole reside in distinct layers [23,24]. Because of the reduced overlap of the electron and hole wave functions, interlayer excitons exhibit longer recombination lifetimes than intralayer

*fadiliyikanat@iyte.edu.tr

excitons [25,26]. On the other hand, spatial separation between the charge carriers of interlayer excitons leads to reduced oscillator strength and binding energy [27]. Therefore, it is difficult to observe interlayer excitons in absorption experiments. Nevertheless, Deilmann *et al.* predicted formation of mixed interlayer excitons, which are composed of intralayer and interlayer excitons in bilayer MoS_2 [28]. They stated that these mixed interlayer excitons exhibit strong and easily tunable optical amplitude.

Herein, motivated by the above studies, stacking-type-dependent excitonic properties of bilayer blue phosphorene are investigated by employing first-principles calculations based on density functional theory (DFT) and many-body perturbation theory (MBPT). The present paper is organized as follows: detailed information about computational methodology is given in Sec. II. The structural properties and electronic band dispersions of bilayer blue phosphorene are given in Sec. III. By solving the Bethe-Salpeter equation on top of a *GW* calculation, optical properties of bilayer blue phosphorene are discussed in Sec. IV. Finally, we conclude our results in Sec. V.

II. COMPUTATIONAL METHODOLOGY

We performed DFT calculations with the Perdew-Burke-Ernzerhof (PBE) exchange-correlation functional as implemented in the QUANTUM ESPRESSO code [29,30]. The pseudopotentials were taken from the Pseudo-Dojo database [31]. Norm conserving pseudopotentials with a kinetic energy cutoff of 60 Ry were used. The van der Waals forces, which have a significant effect on the interlayer distances of the bilayer structures, were included using the DFT-D2 method of Grimme [32]. Periodic images of monolayer and bilayer structures were separated by at least 20 Å of vacuum spacing in the direction normal to the nanosheet plane. We used $18 \times 18 \times 1$ k-point samplings for the primitive unit cells of both monolayer and bilayer structures. The cohesive energy per atom of monolayer and bilayer structures was calculated as $E_{\text{Coh.}} = (nE_s\text{-}E_T)/n$, where E_s, E_T, and n denote the single-atom energy, total energy, and total number of atoms in the unit cell, respectively. The convergence criterion for energy was taken to be 10^{-6} Ry between two consecutive steps. The net force on each atom was reduced to a value of less than 10^{-5} Ry/au.

The DFT eigenvalues were corrected by the G_0W_0 calculation (plasmon-pole approximation) as implemented in the YAMBO code [33–35]. The excitonic effects of monolayer and bilayer blue phosphorene were calculated by solving the Bethe-Salpeter equation (BSE) on top of G_0W_0 [36,37]. The excitations were calculated in terms of electron-hole pairs:

$$(E_{ck} - E_{vk})A^S_{vck} + \sum_{k'v'c'} \langle vck|K_{eh}|v'c'k'\rangle A^S_{v'c'k'} = \Omega^S A^S_{vck}, \quad (1)$$

where E_{vk} and E_{ck} are the quasiparticle energies of the valence and conduction band states, respectively. K_{eh} describes the interaction between excited electrons and holes. A^S_{vck} and Ω^S denote the corresponding exciton eigenfunction and eigenvalue, respectively. Our test calculations showed that convergence of 50 meV of the quasiparticle band gap and optical spectra of monolayer and bilayer structures was reached with 300 bands and $42 \times 42 \times 1$ k-point samplings. Both G_0W_0 and BSE calculations were performed with $42 \times 42 \times 1$ k-point samplings. We used 300 bands for the self-energy and 300 bands for the dynamical dielectric screening in the G_0W_0 step. The Coluomb interaction was truncated at the edges of unit cells in the direction normal to the nanosheet plane [38]. Since we are interested only in the low-energy part of the optical spectra, the four highest valence bands and four lowest conduction bands were included in the calculation of excitonic states.

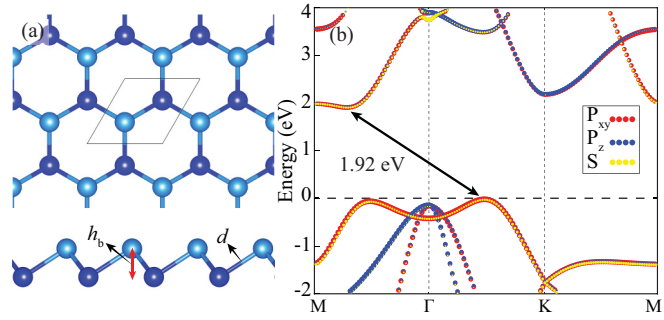

FIG. 1. (a) Top and side views of optimized geometric structures and (b) the orbital-projected electronic band dispersions of monolayer blue phosphorene. The rhombus represents a unit cell of the structure. Light and dark blue atoms show the upper and lower P atoms in the layer, respectively.

III. STRUCTURAL AND ELECTRONIC PROPERTIES OF MONOLAYER AND BILAYER BLUE PHOSPHORENE

A. Monolayer blue phosphorene

As displayed in Fig. 1(a), monolayer blue phosphorene consists of phosphorus atoms arranged in a honeycomb lattice structure. Freestanding monolayer blue phosphorene exhibits a silicene-like buckled structure due to sp^3 hybridization. The optimized lattice constant of monolayer blue phosphorene is found to be 3.28 Å, which is consistent with the previous theoretical studies and 0.2 Å lower than the experimentally observed lattice parameter of the monolayer structure synthesized on a Au(111) surface [15,19]. As given in Table I, the distance between two P atoms is calculated to be $d =$ 2.27 Å. It is found that the buckling thickness of monolayer

TABLE I. Calculated parameters for the monolayer and four different stacking configurations of bilayer blue phosphorene: the lattice constant, a; P-P distance, d; buckling height, h_b; interlayer distance, h_i; the cohesive energy per atom, $E_{\text{Coh.}}$; energy band gap values within GGA and GGA+G_0W_0, E_g^{GGA} and $E_g^{G_0W_0}$, respectively.

	a (Å)	d (Å)	h_b (Å)	h_i (Å)	$E_{\text{Coh.}}$ (eV)	E_g^{GGA} (eV)	$E_g^{G_0W_0}$ (eV)
Monolayer	3.28	2.27	1.24		3.550	1.92	3.36
AA_L	3.28	2.27	1.24	3.24	3.576	1.03	2.337
AA_H	3.28	2.27	1.24	4.12	3.563	1.52	2.965
AB_L	3.28	2.27	1.24	3.22	3.575	1.02	2.348
AB_H	3.28	2.27	1.24	4.06	3.564	1.50	2.939

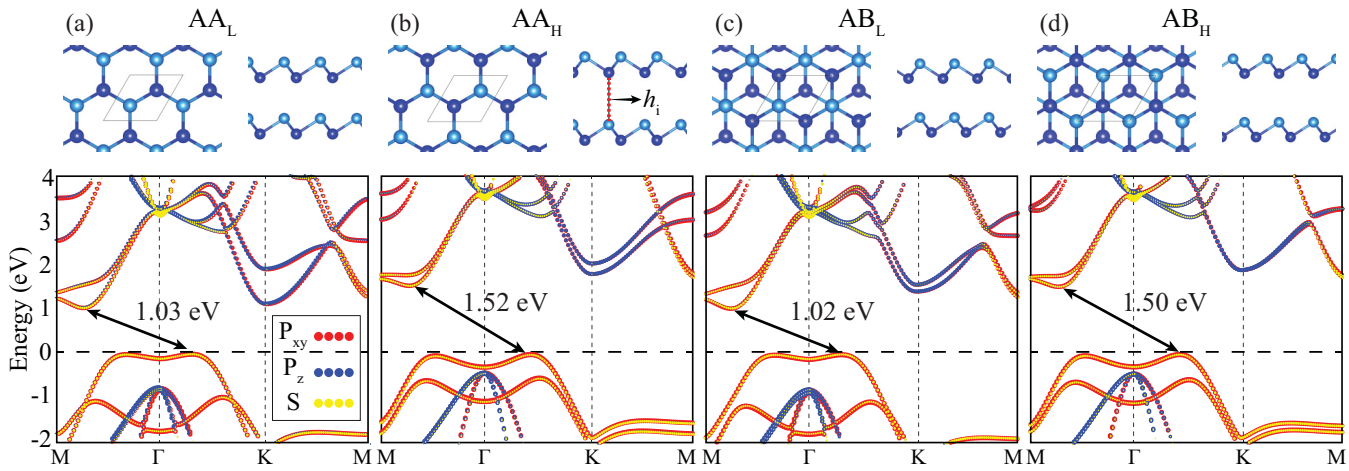

FIG. 2. Top and side views of optimized geometric structures and the orbital projected electronic band dispersions of (a) AA_L, (b) AA_H, (c) AB_L, and (d) AB_H stacked bilayer blue phosphorene. Light and dark blue atoms show the upper and lower P atoms in each layer, respectively.

blue phosphorene, $h_b = 1.24$ Å, is much larger than that of monolayer silicene (0.44 Å). The calculated cohesive energy per atom of monolayer blue phosphorene is 3.55 eV. Previously it was predicted that while the cohesive energies of free-standing monolayer blue phosphorene and black phosphorene are very close, blue phosphorene is found to be more stable energetically than black phosphorene on GaN(011), Au(111), and Cu(111) surfaces [39,40]. The orbital-projected electronic band dispersions of monolayer blue phosphorene are illustrated in Fig. 1(b). The calculated band structure is consistent with the ones previously reported in the literature [19,41]. Monolayer blue phosphorene has an indirect band gap of 1.92 eV with the valence band maximum (VBM) located in between Γ and K points and the conduction band minimum (CBM) in between Γ and M points. Orbital projected band structure reveals that the major contribution to the valence and the conduction band edges originates from the hybridized s and p_{xy} orbitals. Moreover, there is a second valance band edge with the same orbital character as the VBM between the Γ and M points in the Brillouin zone (BZ), being only 42 meV lower in energy than the VBM.

B. Bilayer blue phosphorene

After characterizing the structural and electronic properties of monolayer blue phosphorene, we studied its bilayer forms. It has been reported for several systems that the optical properties, electronic band dispersions and the band gaps of bilayer 2D materials strongly depend on the stacking configuration of the bilayer [42,43]. Therefore, for a thorough examination of the electronic and optical properties of a bilayer material, all possible stacking configurations should be considered. As can be seen in Figs. 2(a)–2(d) there are four different high-symmetry configurations with which to construct bilayer blue phosphorene. According to their stacking type and interlayer distance, we label these bilayers as follows: AA_L, top and bottom layers overlap exactly; AA_H, top and bottom layers overlap but the buckling order between the layers is reversed; AB_L, while the upper atoms of the layers overlap, lower atoms of the top layer are in the middle of the hexagon of the other layer; AB_H, while the lower atoms of the top layer are on top of the upper atoms of the bottom layer, the other atoms are in the middle of the hexagons of the other layer. Table I shows that the lattice constants, interatomic distances, and buckling height of the four bilayer systems are the same as those of monolayer blue phosphorene. On the other hand, the calculated interlayer distance (h_i) varies considerably depending on the type of stacking. While the interlayer distances for AA_L and AB_L are 3.24 and 3.22 Å, respectively, the AA_H and AB_H configurations have almost 1 Å larger interlayer distances (4.12 and 4.06 Å, respectively). In order to predict stabilities, the cohesive energies of the bilayer configurations are also calculated and given in Table I. AA_L stacking ordering is found to be energetically the most favorable configuration. Compared to the AA_H and AB_H stackings, reduction of the interlayer distances increases the interlayer interactions and therefore the cohesive energies in AA_L and AB_L stackings.

The orbital projected electronic band dispersions of different bilayer configurations [see the lower panels of Figs. 2(a)–2(d)] exhibit indirect-gap characteristics similar to those of monolayer blue phosphorene, while the band gaps of bilayers are much lower. The indirect band gaps of AA_L, AA_H, AB_L, and AB_H are calculated to be 1.03, 1.52, 1.02, and 1.50 eV, respectively. It is clear that difference in the interlayer distances due to the stacking type plays an important role in determining the electronic band gap. As the interlayer distance increases the electronic band gap of bilayer increases (see Table I). Similarly to the band structure of monolayer blue phosphorene, dominant configurations for the states of the valance and conduction band edges emerge from the hybridized s and p_{xy} orbitals. In addition, the electronic band dispersions of AA_L (AA_H) and AB_L (AB_H) exhibit very similar behavior except for the K point in the BZ. Compared to the Bernal (AB) stacking, decreased symmetry in the AA stacking leads to splitting of conduction bands around the K point.

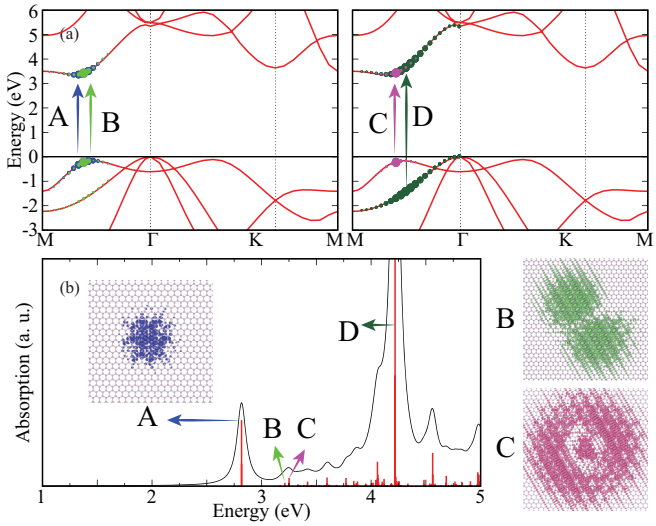

FIG. 3. (a) Electronic band structures within G_0W_0 and (b) optical absorption spectrum and oscillator strengths of monolayer blue phosphorene. The insets show the real space exciton wave functions.

IV. EXCITONIC PROPERTIES OF MONOLAYER AND BILAYER BLUE PHOSPHORENE

A. Monolayer blue phosphorene

The quasiparticle energies of monolayer blue phosphorene are computed by performing a G_0W_0 approximation on top of a DFT calculation and calculated band structure is shown in Fig. 3(a). The G_0W_0 approximation has significant effects on the electronic band structure and increases the indirect band gap of monolayer blue phosphorene from 1.92 to 3.36 eV as the electron-electron interaction is enhanced due to weakly screened Coulomb interaction in 2D structures. Our predicted quasiparticle band gap value of monolayer blue phosphorene is slightly lower than the previously reported value of 3.53 eV [16]. It is found that the inclusion of the G_0W_0 correction not only shifts the band edges but also alters the band dispersions of monolayer blue phosphorene. While the correction has a negligible effect on the dispersion of the conduction bands, the VBM is shifted toward the Γ point. Since the G_0W_0 correction is not uniform in the whole BZ, the scissor shift technique is not suitable for this material.

Although the calculation of the quasiparticle energy is sufficient to get an accurate electronic structure of a material, it is necessary to take into account the electron-hole interactions to obtain the correct optical spectrum. For this purpose, the BSE calculation is performed using the energy eigenvalues obtained from the G_0W_0 calculation; this procedure is proven to be reliable in calculating highly accurate optical properties of 2D materials. Figure 3(b) shows the absorption spectrum of monolayer blue phosphorene obtained using the imaginary part of the dielectric function. Among several excitons located below the indirect band gap of blue phosphorene, we only considered three main bound excitons, A, B, and C, located near the optical band edge with high oscillator strengths. The peak positions of A, B, and C excitons are found to be at 2.817, 3.213, and 3.251 eV, respectively. Our calculations show that the oscillator strength of A is much higher than that of B and C excitons. In Fig. 3(a), the band and the k-point compositions of the indicated excitons are shown. As seen in the figure, all three peaks originate from the same k point in the BZ with the electronic band gap of 3.653 eV. The binding energies of A, B, and C excitons are calculated to be 0.836, 0.440, and 0.402 eV. Comparison with the projected band structure reveals that the these excitons are formed by hybridized s and p_{xy} orbitals. In order to understand the excitonic properties in detail, the real-space excitonic wave functions of the material are calculated using the following formula:

$$\Phi^S(\vec{x}_e, \vec{x}_h) = \sum_{k,v,c} A^S_{vck} \phi_{ck}(\vec{x}_e) \phi^*_{vk}(\vec{x}_h), \tag{2}$$

where S denotes the exciton and A^S_{vck} is the coefficient of the S exciton obtained by the diagonalization of the Bethe-Salpeter equation [36]. ϕ_{ck} and ϕ_{vk} are electron and hole wave functions, respectively. For real-space plots of A, B, and C excitons shown in the inset and side panel of Fig. 3(b), the hole position is fixed near the P atom in the center of the figures and the corresponding electron distributions are shown. It is clear that wave functions of the A, B, and C excitons resemble the $1s$, $2p$, and $2s$ states of the hydrogen atom. As expected, the exciton A is more localized than the B and C excitons. Calculated exciton binding energies, peak positions, and exciton wave functions of monolayer blue phosphorene are very similar to the previously reported values [16]. Furthermore, the most prominent optical transition, is located at the 4.219 eV. Differing from the other excitons, the exciton D is formed by p_z orbitals and hybridized s-p_{xy} orbitals.

B. Bilayer blue phosphorene

The calculated indirect quasiparticle band gaps of AA_L, AA_H, AB_L, and AB_H stacked bilayers of blue phosphorene are 2.337, 2.965, 2.348, and 2.939 eV respectively. Similar to the monolayer case, inclusion of G_0W_0 correction leads to ∼1.44 eV increase in the band gap of the AA_H and AB_H stacked bilayers. However, the G_0W_0 correction for the AA_L and AB_L stacked bilayers (∼1.33 eV) is lower than that of the monolayer. Therefore, increased interlayer interaction with the reduction of interlayer distance in AA_L and AB_L stacked bilayers causes an increase in the screening effect between the layers and a decrease in the band gap correction. Absorption spectra of AA_L, AA_H, AB_L, and AB_H bilayers of blue phosphorene are shown in Figs. 4(a)–4(d), respectively. Similar to the monolayer case, the optical band edge of bilayers consists of various optical transitions. For the sake of simplicity, we focus only on the in two main peaks (E_1 and E_2) near the optical band edge.

Absorption spectrum of AA_L stacked bilayer is shown in the middle panel of Fig. 4(a). The first bright exciton of AA_L, AA_L^{E1}, is at 2.367 eV, which is located at the lowest energy compared to the bright excitons of the other stacking types. The most prominent excitonic peak around the optical gap of AA_L, AA_L^{E2}, is located at 2.701 eV. The oscillator strength of the AA_L^{E1} is significantly lower than that of the AA_L^{E2}. The upper panel of Fig. 4(a) shows that the AA_L^{E1} exciton emerges from the transitions from the highest valance band to the lowest conduction band, whereas the AA_L^{E2} is mainly due to the transitions from the highest valance band to the second

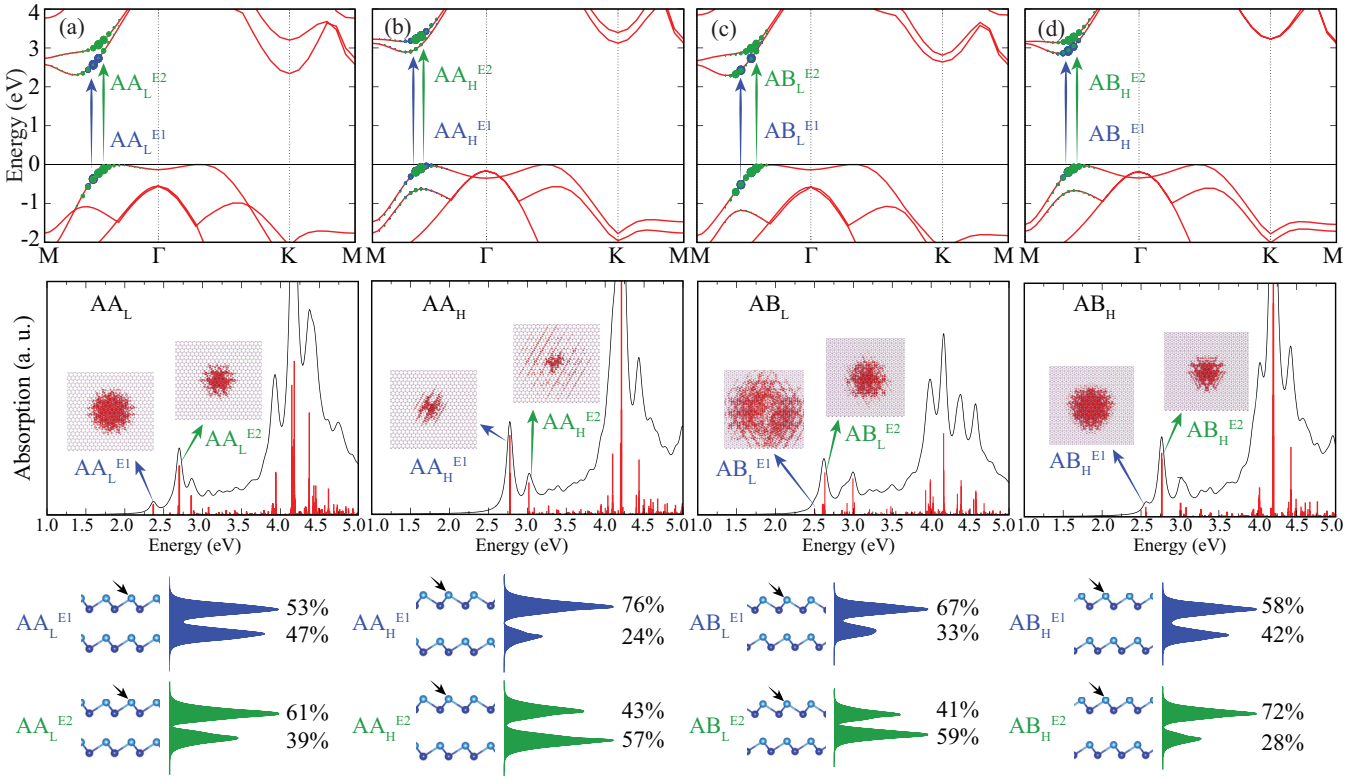

FIG. 4. Electronic band dispersions within G_0W_0 (the upper panels); optical absorption spectra, oscillator strengths, and top views of the real space exciton wave functions (the middle panels); and the percentage of the excitonic wave function on each layer (the bottom panels), of (a) AA_L, (b) AA_H, (c) AB_L, and (d) AB_H stacked bilayer blue phosphorene. In all cases, the hole position is indicated by the black arrow.

conduction band. It also appears that a small contribution comes from the first conduction band to the AA_L^{E2}. Although the oscillator strengths of the AA_L^{E1} and AA_L^{E2} excitons are quite different, their exciton binding energies are close to each other: 0.628 and 0.629 eV, respectively. In order to determine the character of excitons in all bilayer structures examined throughout this study, the real space exciton wave function is calculated by fixing the hole position near the P atom of the upper layer and is shown in the inset of the middle panel of Fig. 4. It is seen that the wave function of the AA_L^{E2} is more localized than that of the AA_L^{E1}. The bottom panel of Fig. 4(a) shows that wave functions of these excitons reside on both layers with similar density, hence they exhibit mixed interlayer exciton character in which intralayer and interlayer excitons are hybridized.

Differing from the AA_L stacking, the lowest exciton peak of the AA_H, AA_H^{E1}, is the most prominent peak around the optical gap. AA_H^{E1} (2.775 eV) and AA_H^{E2} (3.020 eV) peak positions are ∼0.4 and ∼0.3 eV higher than those of the AA_L^{E1} and AA_L^{E2}, respectively. The upper panel of Fig. 4(b) shows that the AA_H^{E1} and AA_H^{E2} excitons are mainly composed of the transitions from the highest valance band to the second conduction band. It is seen from the middle panel of Fig. 4(b) that the oscillator strength of the AA_H^{E2} is almost half that of the AA_H^{E1}. Top views of the wave functions of the AA_H^{E1} and AA_H^{E2} are illustrated in the inset of the middle panel of Fig. 4(b). While the exciton wave function of the AA_H^{E2} spreads widely to the two layers, the wave function of the AA_H^{E1} is more localized and the hole and electron are mostly located on the same layer [see the bottom panel of Fig. 4(b)]. Since the hole is placed on the upper layer, compared to the AA_L configuration increased interlayer distance in the AA_H configuration leads to formation of mostly intralayer excitons. As a result, the exciton binding energy of the AA_H^{E1} (0.633 eV) is much higher than that of the AA_H^{E2} (0.388 eV).

The absorption spectrum of AB_L stacked bilayer blue phosphorene shows that the AB_L^{E1} and AB_L^{E2} excitons are located at 2.503 and 2.634 eV, respectively. As seen in the upper panel of Fig. 4(c), while the AB_L^{E1} is composed of the transitions from the highest valance band to the lowest conduction band, the AB_L^{E2} consists of the transitions from the highest valance band to the first two conduction bands. The middle panel of Fig. 4(c) shows that the oscillator strength of the AB_L^{E1} is very weak compared to the AB_L^{E2}. It is clearly seen that a few excitations with similar oscillator strengths arise near the AB_L^{E2} exciton. Insets in the figure show that the exciton wave function of the AB_L^{E2} is more localized than that of the AB_L^{E1}. The bottom panel of Fig. 4(c) shows that exciton wave functions of both AB_L^{E1} and AB_L^{E2} spread over the two layers and thus exhibit mixed interlayer character. The exciton binding energies of the AB_L^{E1} and AB_L^{E2} are calculated to be 0.488 and 0.644 eV, respectively.

It is found that while the first bright exciton of the AB_H, AB_H^{E1}, is at 2.561 eV, the most prominent peak, AB_H^{E2}, is located at 2.765 eV. The upper panel of Fig. 4(d) shows that the AB_H^{E1} is composed of the transitions from the highest valance band to the lowest conduction band. However, the AB_H^{E2} is composed of the transitions from the highest valance band to

the second conduction band. As shown in the bottom panel of Fig. 4(d), AB_H^{E1} shows mixed interlayer character, while AB_H^{E2} exhibits mostly intralayer character. Exciton binding energies of the AB_H^{E1} and AB_H^{E2} are calculated to be 0.653 and 0.641 eV, respectively.

As a result, detailed analysis of excitonic peaks shows that different stacking types exhibit distinct optical spectra near the optical band edge, allowing identification of the type of the stacking. The strong screening of the substrate does not significantly alter the optical spectrum of the ultrathin materials as it similarly reduces the exciton binding energy and the quasiparticle band gap of 2D materials [6]. Therefore, we expect that the stacking type of the bilayer structure can be determined even in the presence of a substrate. As expected, when the thickness of the material is increased from monolayer to bilayer, a significant decrease in exciton binding energies is determined. Our calculations show that, depending on the type of stacking, the prominent peaks near the optical band edge of bilayer blue phosphorene are composed of mostly intralayer or mixed interlayer excitons. In contrast to interlayer excitons of TMD heterostructures, the mixed interlayer excitons of bilayer blue phosphorene have high oscillator strength and high exciton binding energy due to the greater overlap of the electron and hole wave functions. Moreover, the mixed interlayer excitons of bilayer blue phosphorene have a longer recombination lifetime than the intralayer excitons of monolayer blue phosphorene because of less overlap of electron and hole wave functions.

V. CONCLUSIONS

In conclusion, using first-principles calculations in the framework of MBPT we investigated the electronic and optical properties of monolayer and various bilayer configurations of blue phosphorene. Recently synthesized monolayer blue phosphorene exhibits a large indirect band gap. Electronic structure calculations revealed that band dispersions and the band gap of bilayer blue phosphorene are strongly dependent on the stacking type.

In order to reveal excitonic properties of monolayer and bilayer configurations of blue phosphorene, the Bethe-Salpeter equation was solved on top of G_0W_0 calculations. It was found that the lowest-energy exciton of the monolayer material is bright and has a very high exciton binding energy. It was calculated that the maximum exciton binding energy of bilayer blue phosphorene (0.644 eV) is ∼23% lower than the binding energy of the lowest-energy exciton of the monolayer structure. Depending on the stacking types of bilayer blue phosphorene, mostly intralayer and mixed interlayer excitons were determined near the optical band edge. Unlike the interlayer excitons of the TMD heterostructures, mixed interlayer excitons of bilayer blue phosphorene have high oscillator strengths. Thanks to its high and robust exciton binding energy and controllable optical spectrum, ultrathin blue phosphorene is a promising material for optoelectronic device applications.

ACKNOWLEDGMENTS

Computational resources were provided by TUBITAK ULAKBIM, High Performance and Grid Computing Center (TR-Grid e-Infrastructure). H.S. acknowledges financial support from the Scientific and Technological Research Council of Turkey (TUBITAK) under Project No. 117F095. H.S. acknowledges support from Turkish Academy of Sciences under the GEBIP program.

[1] D. D. Sell, Phys. Rev. B **6**, 3750 (1972).
[2] W. Shan, B. D. Little, A. J. Fischer, J. J. Song, B. Goldenberg, W. G. Perry, M. D. Bremser, and R. F. Davis, Phys. Rev. B **54**, 16369 (1996).
[3] Z. Ye, T. Cao, K. O'Brien, H. Zhu, X. Yin, Y. Wang, S. G. Louie, and X. Zhang, Nature (London) **513**, 214 (2014).
[4] G. Luo, X. Qian, H. Liu, R. Qin, J. Zhou, L. Li, Z. Gao, E. Wang, W.-N. Mei, J. Lu, Y. Li, and S. Nagase, Phys. Rev. B **84**, 075439 (2011).
[5] D. G. W. Parfitt and M. E. Portnoi, J. Math. Phys. **43**, 4681 (2002).
[6] M. M. Ugeda, A. J. Bradley, S.-F. Shi, F. H. da Jornada, Y. Zhang, D. Y. Qiu, W. Ruan, S.-K. Mo, Z. Hussain, Z.-X. Shen, F. Wang, S. G. Louie, and M. F. Crommie, Nat. Mater. **13**, 1091 (2014).
[7] A. Splendiani, L. Sun, Y. Zhang, T. Li, J. Kim, C.-Y. Chim, G. Galli, and F. Wang, Nano Lett. **10**, 1271 (2010).
[8] K. F. Mak, C. Lee, J. Hone, J. Shan, and T. F. Heinz, Phys. Rev. Lett. **105**, 136805 (2010).
[9] L. Li, J. Kim, C. Jin, G. J. Ye, D. Y. Qiu, F. H. da Jordana, Z. Shi, L. Chen, Z. Zhang, F. Yang, K. Watanabe, T. Taniguchi, W. Ren, S. G. Louie, X. H. Chen, Y. Zhang, and F. Wang, Nat. Nanotechnol. **12**, 21 (2017).
[10] G. Zhang, A. Chaves, S. Huang, F. Wang, Q. Xing, T. Low, and H. Yan, Sci. Adv. **4**, eaap9977 (2018).
[11] J.-H. Choi, P. Cui, H. Lan, and Z. Zhang, Phys. Rev. Lett. **115**, 066403 (2015).
[12] Z. Jiang, Z. Liu, Y. Li, and W. Duan, Phys. Rev. Lett. **118**, 266401 (2017).
[13] N. Han, N. Gao, and J. Zhao, J. Phys. Chem. C **121**, 17893 (2017).
[14] J. L. Zhang, S. Zhao, C. Han, Z. Wang, S. Zhong, S. Sun, R. Guo, X. Zhou, C. D. Gu, K. D. Yuan, Z. Li, and W. Chen, Nano Lett. **16**, 4903 (2016).
[15] W. Zhang, H. Enriquez, Y. Tong, A. Bendounan, A. Kara, A. P. Seitsonen, A. J. Mayne, G. Dujardin, and H. Oughaddou, Small **14**, 1804066 (2018).
[16] C. E. P. Villegas, A. S. Rodin, A. Carvalho, and A. R. Rocha, Phys. Chem. Chem. Phys. **18**, 27829 (2016).
[17] L. Z. Liu, X. L. Wu, X. X. Liu, and P. K. Chu, Appl. Surf. Sci **356**, 626 (2015).
[18] W. Zhang and L. Zhang, RSC Adv. **7**, 34584 (2017).
[19] R. B. Pontes, R. H. Miwa, A. J. R. da Silva, A. Fazzio, and J. E. Padilha, Phys. Rev. B **97**, 235419 (2018).
[20] F. Wu, T. Lovorn, and A. H. MacDonald, Phys. Rev. Lett. **118**, 147401 (2017).

[21] H. Yu, G.-B. Liu, J. Tang, X. Xu, and W. Yao, Sci. Adv. **3**, e1701696 (2017).
[22] K. Tran, G. Moody, F. Wu, X. Lu, J. Choi, K. Kim, A. Rai, S. A. Sanchez, J. Quan, A. Singh, J. Embley, A. Zepeda, M. Campbell, T. Autry, T. Taniguchi, K. Watanabe, N. Lu, S. K. Banerjee, K. L. Silverman, S. Kim, E. Tutuc, L. Yang, A. H. MacDonald, and X. Li, Nature (London) **567**, 71 (2019).
[23] P. Rivera, J. R. Schaibley, A. M. Jones, J. S. Ross, S. Wu, G. Aivazian, P. Klement, K. Seyler, G. Clark, N. J. Ghimire, J. Yan, D. G. Mandrus, W. Yao, and X. Xu, Nat. Commun. **6**, 6242 (2015).
[24] Y. Yu, S. Hu, L. Su, L. Huang, Y. Liu, Z. Jin, A. A. Purezky, D. B. Geohegan, K. W. Kim, Y. Zhang, and L. Cao, Nano Lett. **15**, 486 (2015).
[25] M. Palummo, M. Bernardi, and J. C. Grossman, Nano Lett. **15**, 2794 (2015).
[26] B. Miller, A. Steinhoff, B. Pano, J. Klein, F. Jahnke, A. Holleitner, and U. Wurstbauer, Nano Lett. **17**, 5229 (2017).
[27] E. Torun, H. P. C. Miranda, A. Molina-Sánchez, and L. Wirtz, Phys. Rev. B **97**, 245427 (2018).
[28] T. Deilmann and K. S. Thygesen, Nano Lett. **18**, 2984 (2018).
[29] J. P. Perdew, K. Burke, and M. Ernzerhof, Phys. Rev. Lett. **77**, 3865 (1996).
[30] P. Giannozzi, S. Baroni, N. Bonini, M. Calandra, R. Car, C. Cavazzoni, D. Ceresoli, G. L. Chiarotti, M. Cococcioni, I. Dabo, A. Dal Corso, S. de Gironcoli, S. Fabris, G. Fratesi, R. Gebauer, U. Gerstmann, C. Gougoussis, A. Kokalj, M. Lazzeri, L. Martin-Samos, N. Marzari, F. Mauri, R. Mazzarello, S. Paolini, A. Pasquarello, L. Paulatto, C. Sbraccia, S. Scandolo, G. Sclauzero, A. P. Seitsonen, A. Smogunov, P. Umari, and R. M. Wentzcovitch, J. Phys.: Condens. Matter. **21**, 395502 (2009).
[31] M. J. van Setten, M. Giantomassi, E. Bousquet, M. J. Verstraete, D. R. Hamann, X. Gonze, and G.-M. Rignanese, Comput. Phys. Commun. **226**, 39 (2018).
[32] S. Grimme, J. Comput. Chem. **27**, 1787 (2006).
[33] L. Hedin and S. Lundqvist, Solid State Phys. **23**, 1 (1970).
[34] G. Onida, L. Reining, and A. Rubio, Rev. Mod. Phys. **74**, 601 (2002).
[35] A. Marini, C. Hogan, M. Grüning, and D. Varsano, Comput. Phys. Commun. **180**, 1392 (2009).
[36] M. Rohlfing and S. G. Louie, Phys. Rev. B **62**, 4927 (2000).
[37] M. Palummo, O. Pulci, R. Del Sole, A. Marini, P. Hahn, W. G. Schmidt, and F. Bechstedt, J. Phys.: Condens. Matter. **16**, S4313 (2004).
[38] S. Ismail-Beigi, Phys. Rev. B **73**, 233103 (2006).
[39] J. Zeng, P. Cui, and Z. Zhang, Phys. Rev. Lett. **118**, 046101 (2017).
[40] Z. Zhu and D. Tománek, Phys. Rev. Lett. **112**, 176802 (2014).
[41] B. Ghosh, S. Nahas, S. Bhowmick, and A. Agarwal, Phys. Rev. B **91**, 115433 (2015).
[42] J. Dai and X. C. Zeng, J. Phys. Chem. Lett. **5**, 1289 (2014).
[43] J. He, K. Hummer, and C. Franchini, Phys. Rev. B **89**, 075409 (2014).